DOI: 10.1002/ange.201304355

Hollow Nanostructures

General Formation of Complex Tubular Nanostructures of Metal Oxides for the Oxygen Reduction Reaction and Lithium-Ion Batteries**

Genqiang Zhang, Bao Yu Xia, Chong Xiao, Le Yu, Xin Wang, Yi Xie, and Xiong Wen (David) Lou**

Hollow micro- and nanostructures have recently been the focus of tremendous interest because of their great potential in various applications, including catalysis, drug delivery, gas sensors, energy conversion, and storage systems.[1–8] In the past decade, there has been great success in developing effective methods for the synthesis of hollow structures, such as hollow spheres, cubes, and 1D micro-/nanotubes.[8–15] However, most of the hollow structures reported are relatively simple. Hollow structures with higher complexity in terms of structure and composition are expected to offer exciting opportunities for both fundamental studies and practical applications. As an example, multi-shelled hollow structures have been shown to exhibit enhanced lithium storage and gas sensing performance compared to simple hollow structures.[16–18] With this interest, researchers worldwide have recently devoted rapidly increasing efforts on the rational design and synthesis of complex hollow structures.[19–21] In particular, tubular structures (such as micro-/nanotubes) can be regarded as special hollow structures that might inherit benefits from both hollow and 1D structures. Despite great advances in complex hollow structures with isotropic architectures, there has been less development in the fabrication of complex 1D hollow structures. Therefore, it would be highly desirable to develop a simple, but general, strategy to effectively synthesize novel, highly complex 1D hollow structures for different functional materials.

Transition-metal oxides, including binary and mixed oxides, are a family of important functional materials that could find widespread uses, including such applications as electrocatalysts for the oxygen reduction reaction (ORR)[22–24] and as electrode materials for lithium-ion batteries (LIBs) and supercapacitors.[16,18,25–27] It has been widely demonstrated that complex hollow micro-/nanostructures of mixed metal oxides could largely improve their performance.[16–18] On the other hand, 1D hollow micro-/nanostructures have also found promising uses in various applications, including energy conversion and storage systems.[28–30] Hence, the fabrication of transition-metal oxides with a 1D tubular structure would be highly desirable for realizing certain functions. Nevertheless, the simple and general synthesis of transition-metal oxide micro-/nanotubes, especially with complex architectures and controllable compositions, is still considered a challenging task.

Herein, we discuss a facile and general strategy to grow novel complex tube-in-tube hollow structures for many binary and mixed metal oxides. As illustrated in Figure 1, the method involves a simple two-step process. In the first step, carbon nanofibers (CNFs) are dispersed in ethylene glycol (EG) with different metal acetate precursors. After refluxing at an elevated temperature for 2 h, a metal glycolate (MG) layer can be uniformly grown on the surface of the CNFs to form a CNF@MG hybrid structure.[18,31] The preferential deposition of MG on the surface of CNFs is facilitated by the existence of abundant surface functional groups on the CNFs.[32,33] In the second step, the complex tube-in-tube structure can be easily formed during thermal annealing of the CNF@MG composites in air. It is postulated that, during

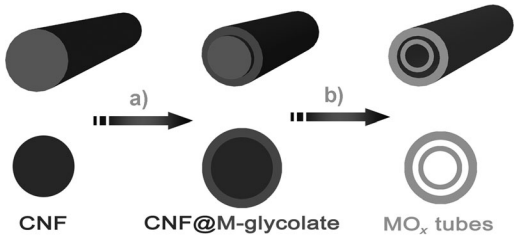

Figure 1. Formation process of metal oxide tube-in-tube complex hollow nanostructures: a) formation of the metal-glycolate coating layer surrounding the surface of the carbon nanofibers (CNFs) through a facile polyol method; b) formation of the complex tube-in-tube structure through a simple thermal annealing treatment in air.

[*] C. Xiao, Prof. Y. Xie
Hefei National Laboratory for Physical Sciences at the Microscale, University of Science and Technology of China
Hefei, Anhui 230026 (P. R. China)
E-mail: yxie@ustc.edu.cn
Dr. G. Q. Zhang, Prof. X. W. Lou
TUM CREATE, 1 CREATE Way, #10-02 CREATE Tower
Singapore 138602 (Singapore)
Dr. G. Q. Zhang, Dr. B. Y. Xia, L. Yu, Prof. X. Wang, Prof. X. W. Lou
School of Chemical and Biomedical Engineering, Nanyang Technological University, 62 Nanyang Drive
Singapore, 637459 (Singapore)
E-mail: xwlou@ntu.edu.sg
Homepage: http://www.ntu.edu.sg/home/xwlou

[**] This publication was made possible by financial support from the Singapore National Research Foundation under its Campus for Research Excellence and Technological Enterprise (CREATE) program.

Supporting information for this article, including detailed experimental procedures, is available on the WWW under http://dx.doi.org/10.1002/anie.201304355.

the annealing process, two different processes with opposite effects could be generated as the temperature increases. One is a contraction process originating from oxidative degradation of the organic species in MG and the CNFs. The other is an adhesive process induced by the gas release that accompanies combustion of the carbon species and, more importantly, the crystallization of metal-oxide crystals that form the solid walls of the tubular structures. To support these two hypotheses, thermogravimetric analysis (TGA) of the CNF@CuCo–glycolate was performed (Supporting Information, Figure S1) and the fraction of organic species contained was estimated to be about 49.3%, in total. Therefore, it is highly possible to generate two processes with opposing effects during the oxidative decomposition of such a large amount of carbon species. After the completion of combustion at a temperature much higher than the decomposition temperature of carbon species from the TGA curves (Figure S1), tube-in-tube structures of phase-pure metal oxides can be obtained.

Figure 2 shows the morphological characterizations of the CNF template and derived structures, using $CuCo_2O_4$ as an example. As shown in Figure 2a, uniform CNFs can be obtained through a Te-nanowire-templated hydrothermal method.[34–36] The inset in Figure 2a shows a typical transmission electron microscopy (TEM) image of the CNFs, which clearly shows the thin hollow cavity in the center of the nanofibers derived from the Te-nanowire template. After refluxing for 2 h, CNF@CuCo–glycolate nanowires can be obtained, as shown in Figure 2b. The 1D morphology is perfectly retained after the reaction, and the diameter increases from about 300 nm for pure CNFs to about 500 nm for the CNF@CuCo–glycolate composite nanofibers. The corresponding TEM image (Figure 2b, inset) reveals the uniform growth of CuCo–glycolate on the surface of the CNFs. Interestingly, there is no clear interface observed from the TEM image between the CNF and the CuCo–glycolate overlayer, suggesting the penetrative growth of CuCo–glycolate into the CNFs. The X-ray diffraction (XRD) pattern of CNF@CuCo-glycoate (Figure S2A) shows no notable difference from that of the CNFs (Figure S2B), which suggests that the as-synthesized CuCo–glycolate is amorphous. After the annealing treatment, the product still retains the large-scale 1D morphology, as revealed by the panoramic field-emission scanning electron microscopy (FESEM) image (Figure 2c). The corresponding XRD pattern (Figure S2C) of the product can be readily indexed to a spinel $CuCo_2O_4$ structure (JCPDS card no. 78-2177), thus indicating the phase purity of the product. The interesting tube-in-tube structure can be clearly identified from both FESEM and TEM images. The inset in Figure 2c shows a typical open end of the $CuCo_2O_4$ tubular structures, which reveals the interesting tube-in-tube structure. The morphological feature can be further confirmed through TEM analysis (Figure 2d). Both closed and open ends of tube-in-tube structures are observed (Figure 2e,f). The average diameter of the outer tubes is about 400 nm, whereas that of the inner tubes is generally in the range of 150–200 nm. Compared to the CNF@CuCo–glycolate nanowires, the diameter of these $CuCo_2O_4$ tube-in-tube nanostructures is reduced, which is caused by overall shrinkage during the annealing process. More interestingly, under TEM anaylsis, some of the $CuCo_2O_4$ tubular structures can even be seen to form more complex triple-layered tube-in-tube structures, as shown in Figure 2g,h. As described above, this $CuCo_2O_4$ tube-in-tube structure can be obtained in large scale and high yield with the simple two-step method.

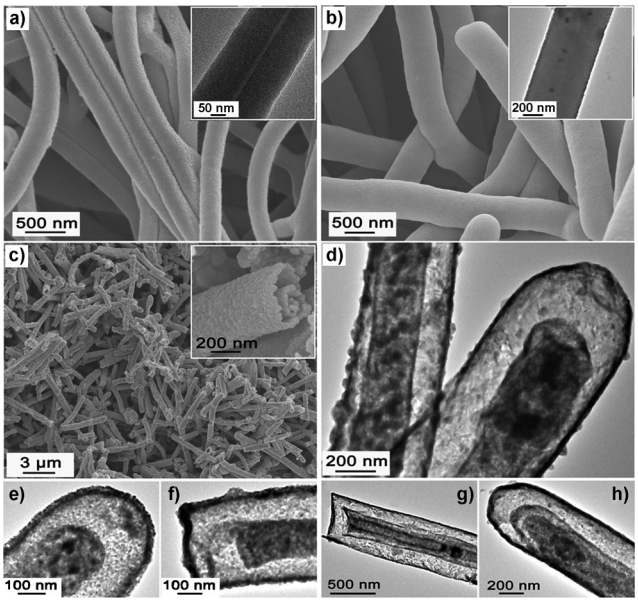

Figure 2. a) Typical FESEM image of the carbon nanofibers (inset: TEM image). b) FESEM image of the CuCo–glycolate-coated carbon nanofibers (inset: TEM image). c) Low-magnification FESEM and d) typical TEM images of $CuCo_2O_4$ complex tube-in-tube structures, the inset in (c) shows an enlarged view of an individual tube-in-tube structure. e,f) Magnified TEM images of the $CuCo_2O_4$ complex tube-in-tube structures. g,h) TEM images of $CuCo_2O_4$ triple-layered tubular structures.

Importantly, the strategy described above is quite general. We have successfully synthesized many other mixed metal oxide tube-in-tube structures. Figure 3 shows typical FESEM and TEM images of $ZnCo_2O_4$ (Figure 3a–c), $CoMn_2O_4$ (Figure 3d–f), $ZnMn_2O_4$ (Figure 3g–i), and $NiCo_2O_4$ (Figure 3j–l) complex tubular structures. As can be seen, similar tube-in-tube structures can be synthesized in large scale and high yield for these four different mixed metal oxides. Their corresponding XRD patterns (Figure S3) can all be well indexed to the respective phases without any impurity peaks. There is some slight difference in the surface roughness of the structures for different materials. For example, the surface of $ZnCo_2O_4$ and $NiCo_2O_4$ tube-in-tube structures is quite rough, whereas that of the $CoMn_2O_4$ and $ZnMn_2O_4$ structures appears relatively smooth. This difference could originate from the different crystallization and crystal growth behavior of different materials during the annealing process. Aside from the aforementioned ternary oxides, the method can be readily extended to synthesize mixed metal oxides with other atomic ratios of the two metal elements involved. As an example, the phase-pure $MnCo_2O_4$ tube-in-tube structures (Figure S4) can be fabricated by simply adjusting the molar ratio of the Mn and Co precursors in the EG solution. This is very useful for the design of materials with controllable compositions for different applications. Our strategy can also

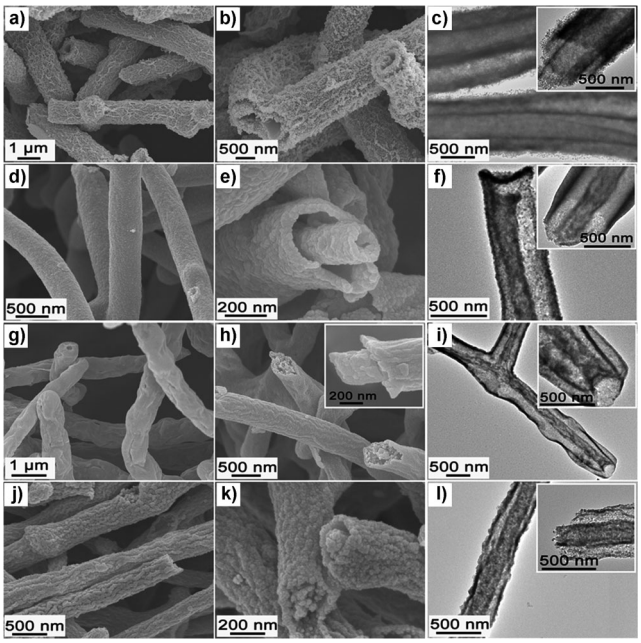

Figure 3. Typical FESEM and TEM images of complex tube-in-tube structures. a–c) $ZnCo_2O_4$, d–f) $CoMn_2O_4$, g–i) $ZnMn_2O_4$, j–l) $NiCo_2O_4$.

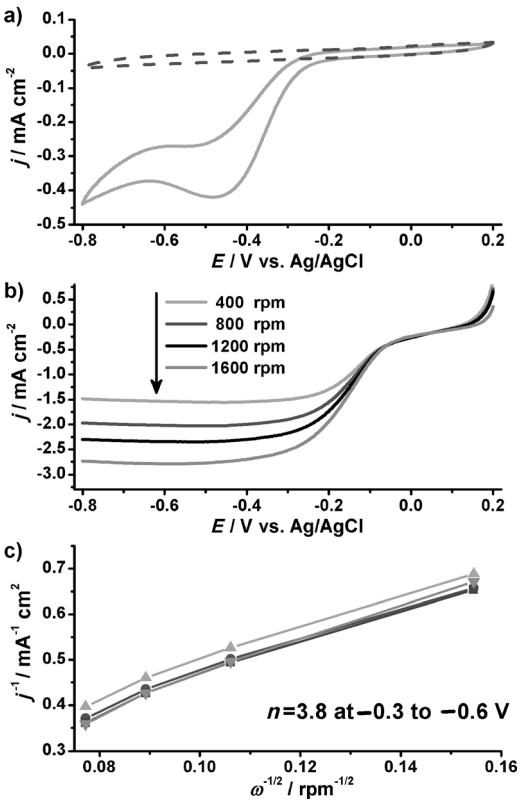

Figure 4. a) CV curves of $MnCo_2O_4$ tube-in-tube structures on an Ar-saturated (-----) and O_2-saturated (——) glassy carbon electrode in KOH solution (0.1 M) with a sweep rate of 50 $mV s^{-1}$. The catalyst loading is about 0.4 $mg cm^{-2}$. b) RDE curves of $MnCo_2O_4$ tube-in-tube structures in O_2-saturated KOH solution (0.1 M) with a sweep rate of 10 $mV s^{-1}$ at different rotation speeds (400–1600 rpm). c) Corresponding Koutecky-Levich plots (j^{-1} vs. $\omega^{-1/2}$) at potentials of −0.6–−0.3 V from the RDE curves shown in (b).

be easily applied to synthesize tube-in-tube structures of various binary metal oxides, such as Mn_2O_3, Co_3O_4, NiO, and Fe_2O_3, with high phase purity and morphological yield (Figures S5–S7). Therefore, this strategy is very effective and versatile for the construction of complex tubular nanostructures for many binary and mixed metal oxide materials.

Mixed metal oxides with a spinel crystal structure are a class of functional materials that could find widespread applications.[24,25,27,37,38] First, we examine the electrocatalytic activity of $MnCo_2O_4$ tube-in-tube structures for the oxygen reduction reaction (ORR). Figure 4a shows the cyclic voltammetry (CV) curves measured in an aqueous KOH solution (0.1M) at room temperature. A comparison of CV curves in O_2- versus Ar-saturated electrolytes reveals the notable ORR electrocatalytic activity of the $MnCo_2O_4$ tube-in-tube structure. Specifically, it exhibits an ORR onset potential of about −0.23 V (vs. Ag/AgCl), and the peak current appears at about −0.43 V. The ORR kinetics were further investigated using a rotating disk electrode (RDE) in a KOH solution (0.1M) under various rotation speeds with a sweep rate of 10 $mV s^{-1}$, as shown in Figure 4b. The current density at −0.23 V is 1.336–2.035 $mA cm^{-2}$ when the rotation speed increases from 400 rpm to 1600 rpm. The limiting current densities are 1.48, 1.99, 2.36, and 2.78 $mA cm^{-2}$ at rotation speeds of 400, 800, 1200, and 1600 rpm, respectively. The limiting current density of these complex metal oxide tubular structures without any carbon additive is remarkable, and is much higher than that in previous reports;[39] it is even comparable to that of $MnCo_2O_4$/graphene hybrid materials in KOH solution (1M).[24] The electron-transfer number (n) is derived from the slopes of Koutecky–Levich plots at various potentials (Figure 4c). The n value was calculated to be approximately 3.8 throughout the investigated potential range of −0.3–−0.6 V, which suggests that a four-electron reduction mechanism is involved.

Mixed metal oxides have also been considered as promising electrode materials for electrochemical energy storage devices, including LIBs and supercapacitors.[16,18,27] We have therefore investigated the lithium storage properties of these tube-in-tube structures, using $ZnCo_2O_4$ as an example. Figure 5a shows representative discharge–charge voltage profiles for the first two cycles. Notably, an initial discharge plateau at around 0.9 V (vs. Li/Li^+) contributes to the majority of the discharge capacity in the first cycle, which shifts to higher voltage and becomes less well-defined in the second cycle. Meanwhile, poorly defined charge plateaus appear in the range of 1.5–2.5 V, and are stable in the first two cycles. Such mixed metal oxides can reversibly react with lithium, presumably based on the conversion reaction mechanism, giving rise to very high lithium storage capacity.[16,18,27] The initial discharge capacity is as high as 1161 $mA h g^{-1}$ for the $ZnCo_2O_4$ tube-in-tube structures, whereas the corresponding charge capacity is 876 $mA h g^{-1}$. The irreversible capacity loss of the first cycle is partly attributed to the initial formation of the solid-electrolyte interface (SEI) film.[40–43] Figure 5b gives the cycling performance of the $ZnCo_2O_4$ electrode at a constant current density 200 $mA g^{-1}$. The capacity gradually decreases from 903 $mA h g^{-1}$ for the

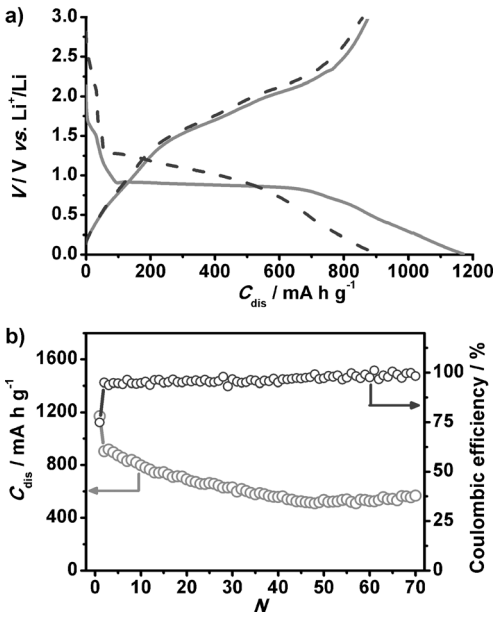

Figure 5. a) Discharge–charge voltage profiles of $ZnCo_2O_4$ tube-in-tube structures. 1st cycle (——), 2nd cycle (-----). b) Cycling performance and Coulombic efficiency (current density = 200 mA g^{-1}) of $ZnCo_2O_4$ tube-in-tube structures.

second cycle to around 560 mA h g^{-1} for the 50th cycle, and stabilizes afterwards. The Coulombic efficiency of the $ZnCo_2O_4$ electrode (Figure 5b) is about 75% in the first cycle, which is considered quite high for transition-metal-oxide-based electrodes. The value quickly increases to around 95% for the second cycle, and reaches 98% after several cycles, thus indicating the good reversibility of the electrode.

In summary, we have developed an effective strategy for the general synthesis of complex tubular structures. In this method, the uniform penetrative growth of the metal-glycolate precursors into the carbon nanofiber template is mainly responsible for the subsequent formation of complex tubular structures upon thermal annealing. Novel tube-in-tube nanostructures have been successfully synthesized for many binary and ternary metal oxides, including $CuCo_2O_4$, $ZnCo_2O_4$, $CoMn_2O_4$, $ZnMn_2O_4$, $MnCo_2O_4$, $NiCo_2O_4$, Mn_2O_3, Co_3O_4, NiO, and Fe_2O_3. We have also demonstrated the promising use of these interesting tubular structures of mixed metal oxides as electrocatalysts for the oxygen reduction reaction and as negative electrodes for lithium-ion batteries.

Received: May 21, 2013
Published online: July 4, 2013

Keywords: electrochemistry · lithium-ion batteries · metal oxides · nanostructures · oxygen reduction reaction

[1] X. W. Lou, L. A. Archer, Z. C. Yang, *Adv. Mater.* **2008**, *20*, 3987.
[2] F. Caruso, R. A. Caruso, H. Mohwald, *Science* **1998**, *282*, 1111.
[3] J. Hu, M. Chen, X. S. Fang, L. W. Wu, *Chem. Soc. Rev.* **2011**, *40*, 5472.
[4] J. Liu, S. Z. Qiao, J. S. Chen, X. W. Lou, X. R. Xing, G. Q. Lu, *Chem. Commun.* **2011**, *47*, 12578.
[5] X. Y. Lai, J. E. Halpert, D. Wang, *Energy Environ. Sci.* **2012**, *5*, 5604.
[6] F. Xie, M. Z. Qi, W. J. Li, K. Wang, Z. Y. Yu, B. Liu, *Prog. Chem.* **2011**, *23*, 2522.
[7] B. Y. Xia, H. B. Wu, X. Wang, X. W. Lou, *J. Am. Chem. Soc.* **2012**, *134*, 13934.
[8] Z. Y. Wang, D. Y. Luan, F. Y. C. Boey, X. W. Lou, *J. Am. Chem. Soc.* **2011**, *133*, 4738.
[9] G. Q. Zhang, W. Wang, Q. X. Yu, X. G. Li, *Chem. Mater.* **2009**, *21*, 969.
[10] L. Z. Wang, F. Q. Tang, K. Ozawa, Z. G. Chen, A. Mukherj, Y. C. Zhu, J. Zou, H. M. Cheng, G. Q. Lu, *Angew. Chem.* **2009**, *121*, 7182; *Angew. Chem. Int. Ed.* **2009**, *48*, 7048.
[11] G. Q. Zhang, Q. X. Yu, Z. Yao, X. G. Li, *Chem. Commun.* **2009**, 2317.
[12] H. Jin fan, M. Knez, R. Scholz, K. Nielsch, E. Pippel, D. Hesse, M. Zacharias, U. Gosele, *Nat. Mater.* **2006**, *5*, 627.
[13] B. Wang, J. S. Chen, H. B. Wu, Z. Y. Wang, X. W. Lou, *J. Am. Chem. Soc.* **2011**, *133*, 17146.
[14] Y. D. Yin, R. M. Rioux, C. K. Erdonmez, S. Hughes, G. A. Somorjai, A. P. Alivisatos, *Science* **2004**, *304*, 711.
[15] X. Wang, W. Tian, T. Zhai, C. Zhi, Y. Bando, D. Golberg, *J. Mater. Chem.* **2012**, *22*, 23310.
[16] L. Zhou, D. Zhao, X. W. Lou, *Adv. Mater.* **2012**, *24*, 745.
[17] Z. H. Dong, X. Y. Lai, J. E. Halpert, N. L. Yang, L. X. Yi, J. Zhai, D. Wang, Z. Y. Tang, L. Jiang, *Adv. Mater.* **2012**, *24*, 1046.
[18] G. Zhang, L. Yu, H. B. Wu, H. E. Hoster, X. W. Lou, *Adv. Mater.* **2012**, *24*, 4609.
[19] M. Yang, J. Ma, C. L. Zhang, Z. Z. Yang, Y. F. Lu, *Angew. Chem.* **2005**, *117*, 6885; *Angew. Chem. Int. Ed.* **2005**, *44*, 6727.
[20] X. Y. Lai, J. Li, B. A. Korgel, Z. H. Dong, Z. M. Li, F. B. Su, J. A. Du, D. Wang, *Angew. Chem.* **2011**, *123*, 2790; *Angew. Chem. Int. Ed.* **2011**, *50*, 2738.
[21] Z. Y. Wang, L. Zhou, X. W. Lou, *Adv. Mater.* **2012**, *24*, 1903.
[22] H. L. Wang, Y. Yang, Y. Y. Liang, G. Y. Zheng, Y. G. Li, Y. Cui, H. J. Dai, *Energy Environ. Sci.* **2012**, *5*, 7931.
[23] J. Du, Y. D. Pan, T. R. Zhang, X. P. Han, F. Y. Cheng, J. Chen, *J. Mater. Chem.* **2012**, *22*, 15812.
[24] Y. Y. Liang, H. L. Wang, J. G. Zhou, Y. G. Li, J. Wang, T. Regier, H. J. Dai, *J. Am. Chem. Soc.* **2012**, *134*, 3517.
[25] F. M. Courtel, H. Duncan, Y. Abu-Lebdeh, I. J. Davidson, *J. Mater. Chem.* **2011**, *21*, 10206.
[26] G. Q. Zhang, H. Bin Wu, H. E. Hoster, M. B. Chan-Park, X. W. Lou, *Energy Environ. Sci.* **2012**, *5*, 9453.
[27] G. Zhang, X. W. Lou, *Adv. Mater.* **2013**, *25*, 976.
[28] X. B. Zhao, X. H. Ji, Y. H. Zhang, T. J. Zhu, J. P. Tu, X. B. Zhang, *Appl. Phys. Lett.* **2005**, *86*, 062111.
[29] L. F. Liu, E. Pippel, *Angew. Chem.* **2011**, *123*, 2781; *Angew. Chem. Int. Ed.* **2011**, *50*, 2729.
[30] T. Song, H. Cheng, H. Choi, J.-H. Lee, H. Han, D. H. Lee, D. S. Yoo, M.-S. Kwon, J.-M. Choi, S. G. Doo, H. Chang, J. Xiao, Y. Huang, W. I. Park, Y.-C. Chung, H. Kim, J. A. Rogers, U. Paik, *ACS Nano* **2012**, *6*, 303.
[31] X. Wang, X. L. Wu, Y. G. Guo, Y. T. Zhong, X. Q. Cao, Y. Ma, J. N. Yao, *Adv. Funct. Mater.* **2010**, *20*, 1680.
[32] J. Liang, Y. Zheng, J. Chen, J. Liu, D. Hulicova-Jurcakova, M. Jaroniec, S. Z. Qiao, *Angew. Chem.* **2012**, *124*, 3958; *Angew. Chem. Int. Ed.* **2012**, *51*, 3892.
[33] X. M. Sun, Y. D. Li, *Angew. Chem.* **2004**, *116*, 607; *Angew. Chem. Int. Ed.* **2004**, *43*, 597.
[34] H. W. Liang, Q. F. Guan, L. F. Chen, Z. Zhu, W. J. Zhang, S. H. Yu, *Angew. Chem.* **2012**, *124*, 5191; *Angew. Chem. Int. Ed.* **2012**, *51*, 5101.
[35] H. W. Liang, W. J. Zhang, Y. N. Ma, X. Cao, Q. F. Guan, W. P. Xu, S. H. Yu, *ACS Nano* **2011**, *5*, 8148.
[36] G. Zhang, L. Yu, H. E. Hoster, X. W. Lou, *Nanoscale* **2013**, *5*, 877.

[37] H. L. Wang, Q. M. Gao, L. Jiang, *Small* **2011**, *7*, 2454.
[38] L. Hu, H. Zhong, X. R. Zheng, Y. M. Huang, P. Zhang, Q. W. Chen, *Sci. Rep.* **2012**, *2*, 986.
[39] M. De Koninck, B. Marsan, *Electrochim. Acta* **2008**, *53*, 7012.
[40] P. Poizot, S. Laruelle, S. Grugeon, L. Dupont, J. M. Tarascon, *Nature* **2000**, *407*, 496.
[41] S. Laruelle, S. Grugeon, P. Poizot, M. Dolle, L. Dupont, J. M. Tarascon, *J. Electrochem. Soc.* **2002**, *149*, A627.
[42] C. M. Ban, Z. C. Wu, D. T. Gillaspie, L. Chen, Y. F. Yan, J. L. Blackburn, A. C. Dillon, *Adv. Mater.* **2010**, *22*, E145.
[43] Y. F. Shi, B. K. Guo, S. A. Corr, Q. H. Shi, Y. S. Hu, K. R. Heier, L. Q. Chen, R. Seshadri, G. D. Stucky, *Nano Lett.* **2009**, *9*, 4215.

